

Magnetic field generation by the Weibel instability at temperature gradients in collisionless plasmas

Yutaka Fujita*

Department of Earth and Space Science,

Graduate School of Science, Osaka University,

Toyonaka, Osaka 560-0043, Japan

Tsunehiko N. Kato

National Astronomical Observatory,

Osawa 2-21-1, Mitaka, Tokyo 181-8588, Japan

Nobuhiro Okabe

Astronomical Institute, Tohoku University, Sendai 980-8578, Japan

(Dated: October 15, 2018)

Abstract

The Weibel instability could be responsible for the generation of magnetic fields in various objects such as gamma-ray bursts, jets from active galactic nuclei, and clusters of galaxies. Using numerical simulations, the development of the Weibel instability at a temperature gradient is studied. It is found that current sheets are first generated at the gradient, and then they are rounded off and turn into current filaments. During this process, return currents are generated around the filaments and they prevent filaments from merger. The magnetic fields around the filaments persist at least until $t \sim 8000/\omega_p$, where ω_p is the plasma frequency, and it is very likely that they survive for a much longer time.

PACS numbers: Valid PACS appear here

*Electronic address: fujita@vega.ess.sci.osaka-u.ac.jp

I. INTRODUCTION

The question of the origin of magnetic fields in the Universe is one of the most challenging problems in modern astrophysics. One of the fascinating ideas is that the fields are generated by the Weibel instability, a plasma instability in a collisionless plasma [1]. This instability is driven by the anisotropy of the particle velocity distribution function (PDF) of plasma. When the PDF is anisotropic, currents and then magnetic fields are generated in the plasma so that the plasma particles are deflected and the PDF becomes isotropic [2]. Through this process, the free energy attributed to the PDF anisotropy is transferred to magnetic field energy. This instability does not need seed magnetic fields. It can be saturated only by nonlinear effects, and thus the magnetic fields can be amplified to very high values. In particular, the generation of magnetic fields at shocks through the instability has been studied by many authors, because the PDF is anisotropic at shocks [2, 3, 4, 5, 6, 7, 8, 9].

However, the magnetic fields generated by the Weibel instability at a shock may not survive for a long time. At a shock, current filaments are created and magnetic fields are generated around them [5, 7]. As the filaments merge together by the magnetic force between them, the magnetic field strength increases [7, 10]. However, the magnetic field should be saturated when the current strength reaches the Alfvén current [11], which is the maximum current allowed by the self-generated magnetic field [12]. The Alfvén current is given by

$$I_A = (mc^3/q)\gamma\beta, \quad (1)$$

where m and q are the mass and charge of a particle, respectively, β is the mean velocity of particles normalized by the speed of light c , and $\gamma = 1/\sqrt{1 - \beta^2}$. After the saturation, magnetic field strength, B , would decrease as the filament size r increases through mergers, because $B \propto I_A/r$ and I_A is constant, although current numerical simulations cannot fully deal with this phase because of the limitation of the simulation box size. The timescale of the filament mergers before the saturation is $\sim 10 \omega_p^{-1}$, where ω_p is the plasma frequency [10]. If the timescale after the saturation is the same as that before the saturation, the magnetic fields would rapidly fade away.

Another site where the Weibel instability could be effective is temperature gradients, where the PDF is also anisotropic [13]. One example of such temperature gradients is cold fronts observed in clusters of galaxies [13, 14]. In this paper, we present the results of numerical simulations of electron-positron plasma performed to investigate the long-term

evolution of the Weibel instability at a temperature gradient. We emphasize that in our simulations, Coulomb collisions are ineffective (collisionless plasma), which is different from the assumption of Ref. [13].

II. MODELS

We performed numerical simulations of an electron-positron plasma at a temperature gradient. The simulation code used is a relativistic, electromagnetic, particle-in-cell code with two spatial and three velocity dimensions, which was developed based on a general description by Ref. [15]. The code is a momentum conserving code. Using the code, we solve the Maxwell equations (in Gaussian units):

$$\frac{1}{c} \frac{\partial \mathbf{E}}{\partial t} = \nabla \times \mathbf{B} - \frac{4\pi}{c} \mathbf{J}, \quad (2)$$

$$\frac{1}{c} \frac{\partial \mathbf{B}}{\partial t} = -\nabla \times \mathbf{E}, \quad (3)$$

$$\nabla \cdot \mathbf{E} = 4\pi\rho, \quad \nabla \cdot \mathbf{B} = 0, \quad (4)$$

where \mathbf{E} is the electric field, \mathbf{B} is the magnetic field, \mathbf{J} is the current density, and ρ is the charge density. We also solve the equation of motion for each particle:

$$\frac{d\mathbf{p}}{dt} = q \left(\mathbf{E} + \frac{\mathbf{p} \times \mathbf{B}}{\gamma m_e c} \right), \quad (5)$$

where \mathbf{p} is the momentum of a particle, and m_e is the electron mass. The simulations are performed on a 1024×512 grid (the axes are labeled as x and y , respectively) with a total of 20 million particles. Temporal and spatial scales in the simulations are normalized to the inverse electron plasma frequency $\omega_p^{-1} = (4\pi n_{e0} e^2 / m_e)^{-1/2}$ and the collisionless skin depth $\lambda_e = c/\omega_p$, where n_{e0} is the average initial electron or positron density, $-e$ is the electron charge, and c is the speed of light, which is the unit of velocity in our simulation code. The units of mass and charge are the electron mass m_e and the absolute value of the electron charge e , respectively. In these normalized units, the box size is 160×80 . For electromagnetic fields, we adopt a periodic boundary condition. For the x direction, we set walls at $x = 20$ and 140 . The regions, $0 < x < 20$ and $140 < x < 160$ are used for Joule

dissipation of electromagnetic waves so that electromagnetic waves do not enter from the other side.

For particles, we adopt a periodic boundary condition for the y direction. On the other hand, for the x direction, we adopt reflection boundary conditions with 'heat walls'. Particles that hit the wall at $x = 20$ have a thermal velocity of $\sigma_L = 0.1$. That is, the reflected particles have the Maxwellian velocity distribution with the deviation of 0.1. At the wall of $x \approx 140$, reflected particles have the one with the deviation of $\sigma_R = 0.5$. For the right wall, we randomly choose the reflection point in $137 < x < 140$ to avoid the formation of artificial structures in the plasma at the wall. Because of these boundary conditions, the total energy of the system does not conserve.

Initially, the plasma in the simulation box has no magnetic fields and is 'isobaric', that is, the square of the thermal velocity ('temperature') times the density is constant. At the left ($x = 20$) and right ($x = 140$) boundaries, the plasma has thermal velocities of $\sigma_L = 0.1$ and $\sigma_R = 0.5$, respectively. For $20 < x < 140$, the temperature changes linearly as x increases. Thus, the density on the left side is higher.

It is to be noted that in another simulation we have calculated the plasma evolution when two plasmas with different temperatures but with the same pressure are bordered at $x = 80$. The results are qualitatively the same as those shown below.

III. RESULTS

Fig. 1 shows the evolution of the magnetic energy, W_B , in units of the total energy in the box at $t = 0$ (the sum of the kinetic energies of all particles). For comparison, the total particle energy, E_P , is shown. The total particle energy decreases because of the cooling at the left wall as well as the generation of magnetic fields.

The magnetic energy rapidly increases at $t \lesssim 400$. Because of the initial density gradient, particles as a whole move in the right direction. In particular, those with large velocities move fast. Thus, on the frame moving with these particles, the effective temperature of the particles is smaller in the x -direction than those of the other directions, which develops the Weibel instability. This initial stage of the instability will be studied in detail elsewhere. Fig. 2 shows the current density in the z -direction (J_z) at $t = 400$. Current sheets are seen at $x \lesssim 80$. Strong magnetic fields are formed around these current sheets. For $x \gtrsim 80$,

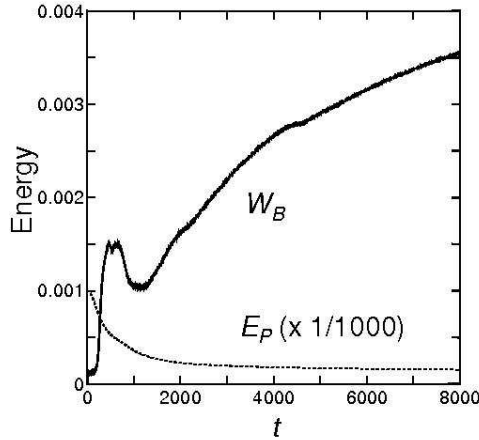


FIG. 1: The evolution of the magnetic energy (W_B : solid) and the total particle energy (E_P : dotted) in units of the total energy in the box at $t = 0$.

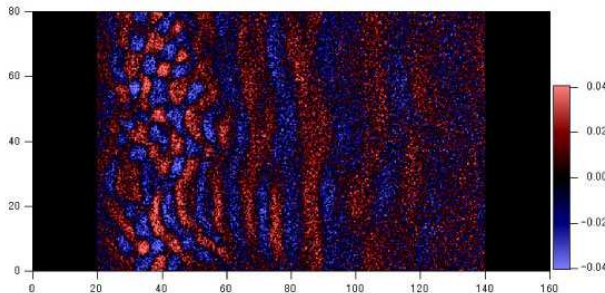


FIG. 2: (Color online). The current density in the z -direction (J_z) at $t = 400$ in units of $n_{e0} ec$.

sheets are still developing. On the other hand, the current density in the x -direction (J_x) is much weaker than J_z and does not contribute to the formation of magnetic fields.

Note that contrary to the Weibel instability at the temperature gradient, current sheets are not created at shocks. While the thermal velocity of particles is larger in the ‘directions’ perpendicular to the temperature gradient in the calculation presented here, it is larger in the ‘direction’ of the shock normal at a shock front [2]. This is the reason why only current

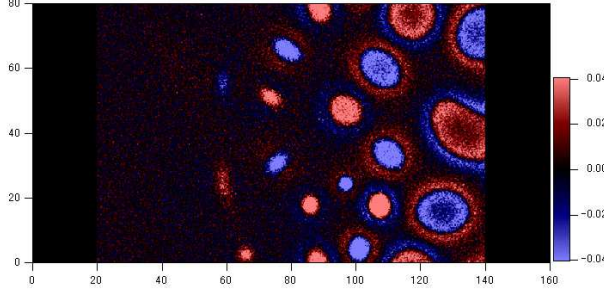


FIG. 3: The same as Fig. 2 but for $t = 5000$.

sheets (two-dimensional structures) are generated in the former. In the latter, only current filaments are formed in the direction of the shock normal.

At $t \sim 400$, W_B reaches its local maximum. We found that the thickness of individual current sheets at $x \lesssim 60$ in Fig. 2 is comparable to the gyroradius of particles. Note that for current filaments, if the radius of the individual filaments is comparable to the gyroradius of particles, the current strength is to be the Alfvén current [11]. It has been shown that the magnetic field strength should reach its maximum at that time [11].

At $650 \lesssim t \lesssim 1100$, the mixing of hot and cold plasmas proceeds, and W_B decreases. However, for $t \gtrsim 1100$, W_B starts increasing again. In this period, the current sheets are rounding and turning into ‘filaments’, because the sheets are unstable. Since the sheets are perpendicular to the temperature gradient, the filaments should also be perpendicular to that direction. In this process, the cross sections of the sheets decrease. The magnetic field strength around the filaments slowly increases through the rounding and shrinking. The increase of the magnetic fields produces electromotive forces around the filaments, which induce return currents around the filaments. The return currents are clearly seen around filaments at $t \gtrsim 1500$ (Fig. 3).

Since the return currents shield the magnetic fields outside the filaments, the magnetic force between the filaments is significantly reduced. At this stage, the filaments stop merging. While the filaments at large x do not evolve, the sheets continue to round at smaller x , and W_B gradually increases even at $t \gtrsim 2000$ (Fig. 1). Fig. 3 also shows that current density is not uniform in a filament. The current density is small at the center of the filament and thus each filament appears to be ‘a current tube’.

In Fig. 3, filaments are seen only at $x \gtrsim 80$. The thermal velocity outside the filaments does not much depend on x and is $\sim \sigma_L = 0.1$. Particles with large velocities come from the

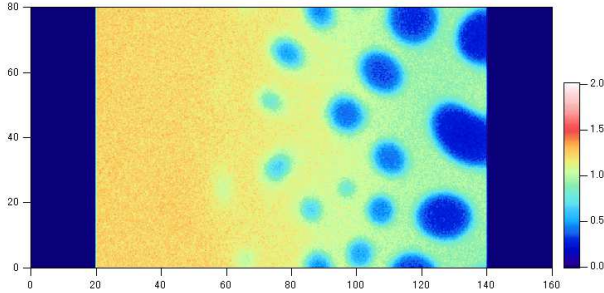


FIG. 4: (Color online). The number density of electrons at $t = 5000$ in units of n_{e0} .

right wall. However, the magnetic field around the filaments prevents those particles from moving to the left wall. Thus, the PDF anisotropy is larger at larger x , which is the reason that filaments develop at larger x .

In our simulations, the particles are merely reflected and redistributed thermally at the right and left walls; they are not uniformly fed into the system. In spite of this, the walls do not create artifacts. This may be because particles in low and high density regions bordered on the same wall are well-separated by magnetic fields and they are not mixed together. It would be interesting to compare the results here with those of the simulations in which particles are uniformly fed into the system.

IV. DISCUSSION

We studied the structure of the stable filaments seen at $x \gtrsim 100$ in Fig. 3. In the filaments close to the right wall, the average drift velocity of particles in the z -direction is $|\beta_{\text{in},z}| \sim 0.05$, while their thermal velocity is $\sigma_{\text{in}} \sim 0.16$. This means that the filaments are ‘hot beams’. Figs. 4 and 5 show the number density and the kinetic energy density of particles at $t = 5000$, respectively. For the filaments at $x \gtrsim 100$, while the number density is small inside them, the kinetic energy density is almost the same between the inside and the outside of the filaments. Fig. 6 shows the magnetic energy density (U_B), and demonstrates that magnetic fields are generated only at the surfaces of the filaments. There is a relation of $U_B = (1/2)(B/B_\star)^2$, where $B_\star = c\sqrt{4\pi n_{e0} m_e}$. The magnetic field strength is determined so that the gyroradius of particles with the velocity of $\sigma_{\text{in}} \sim 0.16$ is comparable to the thickness of the current tubes. This magnetic field confines hot particles within the tubes.

Based on these facts, we can analyze the structure of the magnetic fields as follows. We

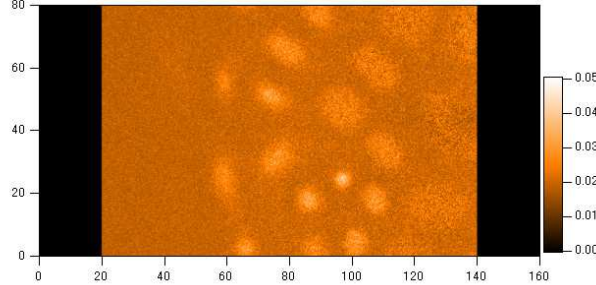


FIG. 5: (Color online). The kinetic energy density of particles (electrons and positrons) at $t = 5000$ in units of $n_{e0}m_ec^2$.

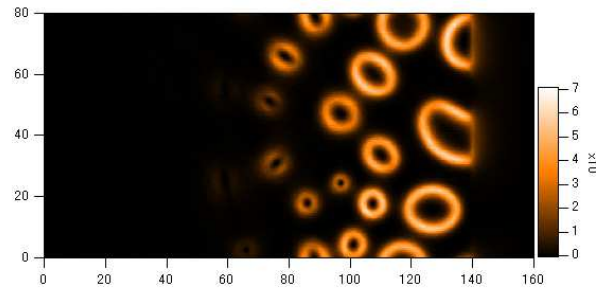


FIG. 6: (Color online). The magnetic energy density, U_B , at $t = 5000$ in units of $n_{e0}m_ec^2$.

use the Gaussian units here. We define ‘thermal pressure’ as

$$P = 2n_e m_e \sigma^2 c^2, \quad (6)$$

where n_e is the density, and σ is the thermal velocity of particles. The factor of two comes from the fact that there are electrons and positrons. Our simulations showed that the thermal velocities inside and outside a filament are $\sigma_{\text{in}} \lesssim \sigma_R$ and $\sigma_{\text{out}} \gtrsim \sigma_L$ ($\sigma_{\text{in}} \gtrsim \sigma_{\text{out}}$), respectively. Fig. 5 suggests that

$$P_{\text{in}} \approx P_{\text{out}}, \quad (7)$$

where P_{in} and P_{out} are the thermal pressures inside and outside a filament, respectively. Equation (7) means that

$$n_{\text{in}} \sigma_{\text{in}}^2 \approx n_{\text{out}} \sigma_{\text{out}}^2, \quad (8)$$

where n_{in} and n_{out} are the electron densities inside and outside a filament, respectively.

Since the gyroradius of particles inside a filament is comparable to the thickness of the

current tube (Δ), the magnetic field strength is given by

$$B \approx \eta \frac{m_e c^2 \sigma_{\text{in}}}{\Delta e}, \quad (9)$$

where η is the ratio of the thickness to the gyroradius. On the other hand, the magnetic field strength is also given by $B = 2I/(rc)$, where I is the current in the filament, and r is the radius of the filament (or the tube). If we assume that the average drift velocity of particles in a filament is given by $|\beta_{\text{in},z}| = \xi \sigma_{\text{in}}$, the current is $I = 4\pi n_{\text{in}} e \beta_{\text{in},z} c r \Delta$. Thus, the magnetic field strength is

$$B = 8\pi \xi n_{\text{in}} e \sigma_{\text{in}} \Delta. \quad (10)$$

Combining equations (8), (9), and (10), we obtain

$$B \approx \sqrt{2\eta\xi} B_{\star} \sigma_{\text{out}}, \quad (11)$$

and

$$\Delta \approx \sqrt{\frac{\eta}{2\xi}} \lambda_e \frac{\sigma_{\text{in}}}{\sigma_{\text{out}}}. \quad (12)$$

We used the relation $n_{\text{out}} \approx n_{e0}$. In our simulations, we observed $\sigma_{\text{in}} = 0.16$, $\sigma_{\text{out}} = 0.08$, and $\xi = 0.3$ for the filaments close to the right wall. For these values and $\eta = 2$, equations (11) and (12) predict that $B/B_{\star} \approx 0.09$ and $\Delta/\lambda_e \approx 4$, which are consistent with the results of the simulations (Fig. 6). The above equations alone cannot determine the radius of a filament r . It may depend on the initial conditions of plasma.

Although we finished the simulations at $t \sim 8000$, we expect that W_B continues to increase for $t \gtrsim 8000$, because of the rounding and shrinking of sheets at smaller x . On the other hand, the filaments at larger x will remain the same. Fig. 7 shows the histogram of $\gamma - 1$ (the kinetic energy of particles in the unit of $m_e c^2$) at $t = 8000$. It shows that particles consist of those with the thermal velocity of $\sim \sigma_L$ and those of $\sim \sigma_R$. A sign of particle acceleration cannot be found.

Our simulations are two-dimensional in space. Thus, we cannot deal with three-dimensional deformations of current filaments, which might be caused by the Kink instability or filament mergers. However, for the mergers, if the time-scale of the formation of return currents is smaller than that of the mergers, the results presented here would not much change. For filaments that have not been shielded by return currents, it would take a longer time to merge together, because the filaments would not be aligned and the magnetic interaction among them would be weaker in a three-dimensional space. Thus, filament mergers

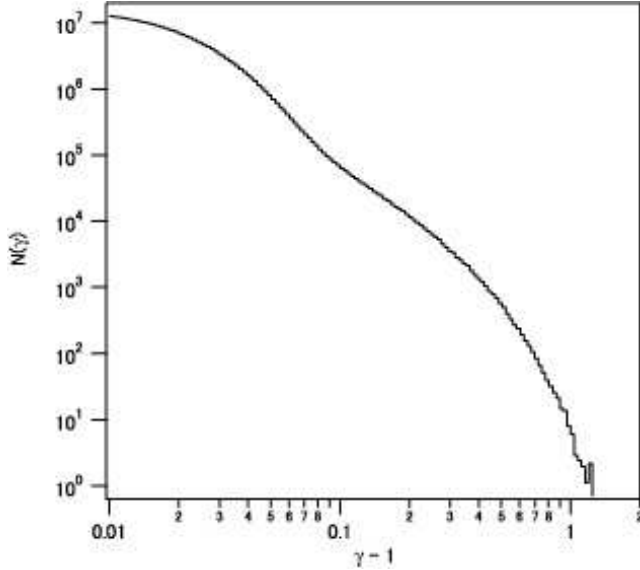


FIG. 7: The histogram of $\gamma - 1$ (the kinetic energy of particles in the unit of $m_e c^2$) at $t = 8000$.

would be further prohibited. On the other hand, while our simulations are two-dimensional in space, they are three-dimensional in velocity space. Therefore, the resultant velocity distribution of particles would not be much different from that in full three-dimensional simulations.

We have shown that magnetic fields generated at a temperature gradient could survive as long as the gradient exists. The essence is the generation of current sheets, which later round and turn into filaments. Return currents created in this process shield the filaments and prevent them from mergers. It would be interesting to study this instability for electron-proton plasma. Assuming that protons and electrons have the same temperature, thermal velocity of the protons is smaller than that of the electrons by a factor of $\sqrt{m_e/m_p}$, where m_p is the proton mass. Since B_* for protons is larger than that for electrons by a factor of $\sqrt{m_p/m_e}$, the resultant magnetic fields would not be much different from that for electron-positron plasma (see Eq. [11]), although it must be confirmed by numerical simulations. It would also be interesting to apply the results to actual objects in the Universe, such as gamma-ray bursts, supernova remnants, and clusters of galaxies. However, the temperature gradients in them are much smaller than that studied in this paper, which might make some difference. Moreover, the coherent scale of the magnetic fields generated by the Weibel instability is much smaller than astrophysical scales. Thus, some mechanisms that increase the scale would be required [8]. In the future, we would like to challenge these problems.

Acknowledgments

Y. F. is supported in part by a Grant-in-Aid from the Ministry of Education, Culture, Sports, Science, and Technology of Japan (17740182).

- [1] E. S. Weibel, Phys. Rev. Lett. **2**, 83 (1959).
- [2] M. V. Medvedev and A. Loeb, Astrophys. J. **526**, 697 (1999).
- [3] Y. Kazimura, J. I. Sakai, T. Neubert, and S. V. Bulanov, Astrophys. J. **498**, L183 (1998).
- [4] K.-I. Nishikawa, P. Hardee, G. Richardson, R. Preece, H. Sol, and G. J. Fishman, Astrophys. J. **595**, 555 (2003).
- [5] L. O. Silva, R. A. Fonseca, J. W. Tonge, J. M. Dawson, W. B. Mori, and M. V. Medvedev, Astrophys. J. **596**, L121 (2003).
- [6] S. Saito and J. I. Sakai, Astrophys. J. **604**, L133 (2004).
- [7] J. T. Frederiksen, C. B. Hededal, T. Haugbølle, and Å. Nordlund, Astrophys. J. **608**, L13 (2004).
- [8] Y. Fujita and T. N. Kato, Mon. Not. R. Astron. Soc. **364**, 247 (2005).
- [9] M. V. Medvedev, L. O. Silva, and M. Kamionkowski, Astrophys. J. **642**, L1 (2006).
- [10] M. V. Medvedev, M. Fiore, R. A. Fonseca, L. O. Silva, and W. B. Mori, Astrophys. J. **618**, L75 (2005).
- [11] T. N. Kato, Phys. Plasmas **12**, 080705 (2005).
- [12] H. Alfvén, Phys. Rev. **55**, 425 (1939).
- [13] N. Okabe and M. Hattori, Astrophys. J. **599**, 964 (2003).
- [14] M. Hattori and N. Okabe, Astrophys. J. **625**, 741 (2005).
- [15] C. K. Birdsall and A. B. Langdon, *Plasma Physics via Computer Simulation* (OP Publishing, Bristol, 1991).